5-2-2022

Optical Vortex Generation Using 3-D Printed Reflection and Transmission Holograms

Tara R. Crowe

Optical Vortex Generation Using 3-D printed Reflection and Transmission Holograms

by

Tara R. Crowe

An Honors Capstone

submitted in partial fulfillment of the requirements

for the Honors Diploma

to

The Honors College

of

The University of Alabama in Huntsville

02 May 2022

Honors Capstone Director: Dr. Don Gregory

Distinguished Professor, Physics and Astronomy

Tara Crowe 05/02/22

Student (signature) Date

Don A Gregory 5/2/22

Director (signature) Date

Tommy Morris 5/2/2022

Department Chair (signature) Date

William Wilkerson Digitally signed by William Wilkerson
Date: 2022.05.03 09:49:48 -05'00'

Honors College Dean (signature) Date

HONORS COLLEGE
THE UNIVERSITY OF ALABAMA IN HUNTSVILLE

Honors College
Frank Franz Hall
+1 (256) 824-6450 (voice)
+1 (256) 824-7339 (fax)
honors@uah.edu

Honors Thesis Copyright Permission

This form must be signed by the student and submitted as a bound part of the thesis.

In presenting this thesis in partial fulfillment of the requirements for Honors Diploma or Certificate from The University of Alabama in Huntsville, I agree that the Library of this University shall make it freely available for inspection. I further agree that permission for extensive copying for scholarly purposes may be granted by my advisor or, in his/her absence, by the Chair of the Department, Director of the Program, or the Dean of the Honors College. It is also understood that due recognition shall be given to me and to The University of Alabama in Huntsville in any scholarly use which may be made of any material in this thesis.

Tara Crowe

Student Name (printed)

Tara Crowe

Student Signature

05/02/22

Date

Table of Contents

Dedication:

This work is dedicated to everyone who has helped me throughout this process, whether by encouraging me, walking me through problems, offering to print holograms for me, letting me use your computer when mine was being slow, or listening to me complain. This wouldn't have been possible without any of you, and I hope you are as proud of this as I am.

Abstract

Computer-generated holograms (CGHs) used to produce optical vortex carrying Laguerre-Gaussian modes are manufactured using three different types of additive manufacturing. Fused Deposition Modeling (FDM), stereolithography (STA), and masked stereolithography (MSLA) 3D printing methods offer convenient and inexpensive alternatives for the fabrication of holographic gratings, although are limited significantly in every case by physically achievable resolutions. The holograms are designed to generate various Laguerre-Gaussian modes by conversion of the fundamental Hermite-Gaussian laser mode and were generated for azimuthal and radial indices of integer values greater than or equal to 0. Testing in transmission showed that large scale holograms manufactured by 3D printing successfully produce Laguerre-Gaussian beams when propagated a large enough distance.

Introduction

An optical vortex is a phase singularity propagated by a beam of light whose phase front spirals about its direction of propagation. The most common example of an optical vortex is that of the Laguerre-Gaussian beam, in which the helical phase front is characterized by an azimuthal phase dependence, known as the Hilbert factor, of $exp(i\ell\phi)$ [1]. The azimuthal angle of the beam, ϕ, is not well defined near the central axis of the helix, and, as a result, the amplitude at those locations vanishes. Such areas of zero amplitude are the previously mentioned phase singularities which appear as dark holes in the center of vortex carrying beams and result in the 'donut' shape typical of helically phased beams.

The principal interest in optical vortices is in the rotation of momentum about the phase singularity and the orbital angular momentum (OAM) such beams carry as a result. Unlike spin angular momentum, OAM is independent of a beam's polarization state [2]. OAM is given by

$$L = \ell\hbar \tag{1}$$

Where ℓ, the same quantity shown in the Hilbert factor, is known as the topological charge of an optical vortex and is indicative of the number and handedness of 2π phase changes which occur in one revolution of ϕ, which some sources interpret to correspond to the velocity of the phase rotation [3] and others [2] as the number of helical phase fronts intertwined within a vortex carrying beam.

The applications of optical vortices are myriad and include particle trapping, optical tweezers, quantum communication, atom cooling, multiplexing in fiber and free-space, high-precision interferometry, and propagation through turbulence. Recent advances in optical vortex technology have focused on increasing the tunability of vortex characteristics including OAM,

wavelength, and chirality, as well as on the generation of optical vortices with fractional topological charge [4].

Optical vortices can appear spontaneously, however their generation typically done via mode conversion of the Hermite-Gaussian (LG) beams which most lasers naturally emit. While Laguerre-Gaussian (LG) modes, the generation of which is the focus of this paper, have been created directly by manipulating optical cavities, they remain easiest to create via external mode conversions achieved using spiral phase plates (SPPs), cylindrical lens systems, or computer-generated holograms (CGHs). SPPs, also known as vortex retarders, offer high conversion efficiency but are difficult to produce and can be expensive to purchase. Cylindrical lens systems also provide highly effective mode conversion but tend to be difficult to align and require specific HG modes to produce each LG mode, limiting their usefulness [2]. Computer generated holograms are by far the most commonly used method to generate vortex beams owing largely to the sheer customizability and ease with which they can be made. Neither can it be argued that CGHs are less effective than the other methods; recent projects have confirmed the efficacy of computer-generated fork holograms in creating high-order LG beams for use in high-power, high-precision interferometers like LIGO Advanced [5,6].

Generally, CGHs are fabricated by processes such as holographic imaging, laser micromachining, and, increasingly, photolithography [7]. Current capabilities of additive manufacturing technologies, however, are such that even hobby quality 3D printers possess resolutions small enough to theoretically print computer-generated fork small enough to successfully generate LG beams. Unlike holographic gratings produced by traditional methods which can maximize diffraction to specific indices by adjusting groove depth or by blazing [8], fork holograms manufactured via 3D printing would, by necessity, be binary transmission

gratings. Despite this, the convenience inherent in producing holograms via 3D printing offers strong motivation to investigate such a method's feasibility, as is explored throughout the rest of this paper.

Chapter 1: Fork Holograms and LG modes

Computer-generated holograms are created by simulating the interference patterns between varying object and reference waves, through which information about the amplitude and phase of both participating waves is recorded. When a pattern is illuminated by one of its constituent waves, the information encoded in the shape of the pattern is imparted such that the wave leaving the hologram is the reconstruction of the other constituent wave. CGHs which result in the production of Laguerre-Gaussian beams, commonly called 'fork' holograms, are created in a similar manner, in which the desired LG mode is taken to be the object wave and a tilted plane wave is taken to be the reference. The azimuthal phase dependence of the LG beam results in a 'forked' central fringe in an otherwise approximately equidistant fringe pattern. The number of extra fringes produced at the bifurcation point of the fork is equivalent to the topological charge of the LG beam minus 1. LG beams with radial mode indices of $p > 0$ result in ring dislocations centered on the bifurcation point of the center fringe, the number of which is equal to the value of p.

Figure 1. Example fork holograms for, from left to right, LG10 (ℓ=1, p=0), LG20 (ℓ=2, p=0), and LG11 (ℓ=1, p=1).

When a fork hologram is illuminated by a plane wave, the resulting Fraunhofer (far-field) diffraction pattern will possess an optical vortex at each order of diffraction maxima, save for the zeroth which consists of light not diffracted by the hologram. For holograms illuminated by a beam with $\ell = 0$, the optical vortex diffracted to each maximum will have a topological charge

of $m = \ell n$ in which n is the diffraction order and ℓ is the topological charge of the hologram (equal to the topological charge of the LG beam from which it was generated) [9]. The handedness a vortex's rotation for positive values of m is the same of the handedness of the original and opposite for those occurring at negative orders.

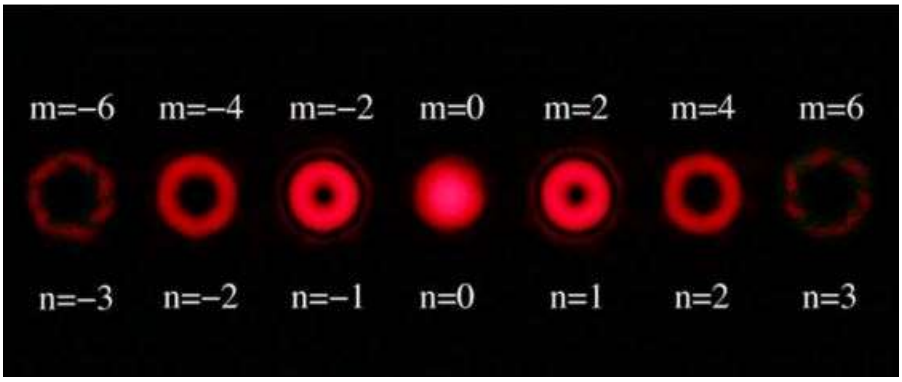

Figure 2. Resulting diffraction pattern from a fork hologram with a topological charge of ℓ=1, and the resulting topological charge of vortices at each diffraction order n [3].

Design and Simulation of Forked Holograms

The Laguerre-Gaussian modes represent a complete set of solutions to the paraxial wave equation. The general form of an LG beam of radial mode p and topological charge ℓ propagating in the z-direction is given, in polar coordinates, by the equation

$$u_p^{\ell}(r,\phi,z) = C_{\ell p}^{LG}\left(\frac{w_0}{w(z)}\right)\left(\frac{r\sqrt{2}}{w(z)}\right)^{|\ell|} exp\left(-\frac{r^2}{w^2(z)}\right) L_p^{\ell}\left(\frac{2r^2}{w^2(z)}\right) \times exp\left(-ik\frac{r^2}{2R(z)}\right) exp(-i\ell\phi) exp\big(i\psi(z)\big) \quad (2)$$

Where

$k = \frac{2\pi}{\lambda}$ is the wave number for wavelength λ,

$C_{\ell p}^{LG}$ is the normalization constant,

w_0 is the beam waist and $w(z)$ is the beam size at z,

$L_p^{\ell}(x)$ are the relevant Laguerre polynomials,

$z_R = \frac{\pi w_0^2}{\lambda}$ is the Rayleigh range,

$R(z) = z\left[1 + \left(\frac{z}{z_R}\right)^2\right]$ is the Radius of curvature, and

$\psi(z) = (zp + \ell + 1)tan^{-1}\left(\frac{z}{z_R}\right)$ is the Gouy phase shift

When modeling interference with such an LG beam, allowing the interference to occur at $z = 0$ and disregarding the normalization constant simplifies Equation (2) significantly to

$$u_p^\ell(r, \phi, z) = \left(\frac{r\sqrt{2}}{w}\right)^{|\ell|} L_p^\ell\left(\frac{2r^2}{w^2}\right) exp\left(-\frac{r^2}{w^2}\right) exp(-i\ell\phi) \quad (3)$$

Where w is now simply the diameter of the beam at the location where the interference is said to occur. The case where $\ell = \mathrm{p} = 0$ represents the fundamental Gaussian solution.

The tilted plane wave which serves as the hologram's reference wave is given by

$$\psi_{ref} = exp\left[i\left(\frac{2\pi x}{\lambda}\right) tan(\theta)\right] \quad (4)$$

Where θ is the angle the plane wave makes with respect to the object wave's direction of propagation. For a desired grating period, the tilt angle θ of the reference wave will equal diffraction angle $\theta_{m\pm1}$ and can be found using the grating equation

$$sin\theta_m = sin\theta_i + m\frac{\lambda}{\Lambda} \quad (5)$$

For wavelength λ, period Λ, and incident angle $\theta_i = 0$.

The interference pattern between LG object wave and tilted plane wave is simulated by taking the algebraic sum of the two waves, for which the absolute value of the result squared is proportional to the resulting irradiance distribution. Binarizing this irradiance distribution results in the inverse of the desired transmission fork hologram. A hologram created from a tilted plane wave and normally incident object wave will function the same in reflection as it does in

transmission, though future iterations of this project may desire to explore situations in which this is not necessarily the case.

Once a hologram has been generated, its far-field diffraction pattern can by simulated by taking its Fast Fourier Transform (FFT), however the low resolution of the results, even with compensation via the technique of zero-padding, warrants the use of an alternate technique where an $e^{i\pi}$ phase shift term is introduced to hologram before the FFT process (see the code in Appendix 1 for more details). The diffraction patterns simulated through this alternate method do not show the 0^{th} order as is present in the experimental results of the holograms, though the higher quality of the simulated orders is a more than acceptable trade off. The basic process this project used to produce fork holograms and simulate diffractions patterns is shown below in figure 3.

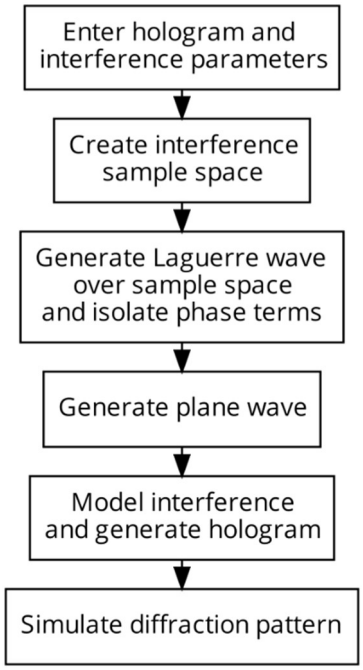

Figure 3. Flow chart of MATLAB program written to generate fork holograms and simulate their diffraction patterns. Full program in Appendix 1.

All holograms generated for this project were done so with the specifications to produce a grating period of $120\ \mu m$ (i.e., an individual fringe width of $60\ \mu m$) and approximately 40 fringe pairs. To create the desired $120\ \mu m$ period, the planar reference wave was given a tilt angle of approximately $\theta = 0.302°$. The wavelength used for all calculations was $\lambda = 632.8\ nm$, typical of Helium-Neon (He-Ne) lasers like those found in UAH's interferometry and turbulence labs. Holograms were generated for square pixel-grids of size 4800x4800 for a 1:1 pixel-to-micron scale. As the desire was to fabricate the gratings using additive manufacturing, a 600-pixel border was added to contain each grating, for a final hologram of size of 6000x6000 pixels, or equivalently 6000x6000 μm. LGℓp beams were generated for LG10, LG20, LG11, LG12, and LG02 modes. For each mode LG11, LG12, and LG02, holograms were created for incident beam diameters of 500λ, 1000λ, and 2000λ, though due to time constraints and hardware issues, only the 1000λ versions were modeled and sent for production.

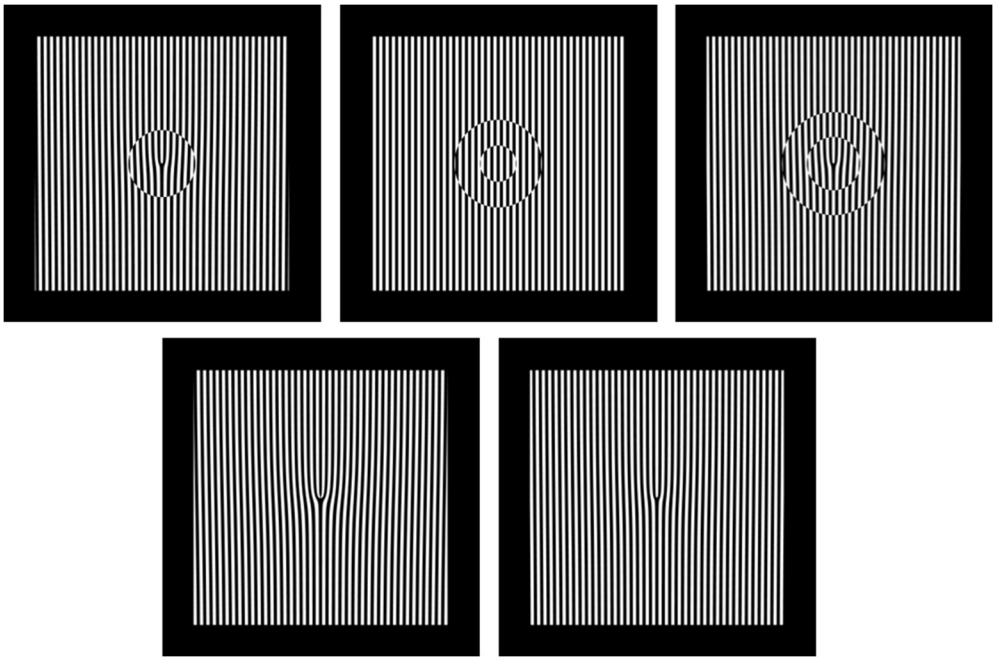

Figure 4. Each grating selected for 3D modeling. Top row consists of modes (from left to right) LG11, LG02, and LG12. Bottom row consists of modes (from left to right) LG20 and LG10.

Chapter 2: The 3D Printing Process

Additive manufacturing has become a staple method for part prototyping and fabrication in many fields due to its convenience and low cost. The 3D printing methods of fused deposition modeling (FDM) and vat polymerization can be used to fabricate various optical devices, including lenses and diffraction gratings [10], though the latter method is generally preferred in deference to the higher resolution its devices are capable of. Vat polymerization printing methods like Stereolithography (SLA) and Digital Light Processing (DLP) work in similar manners by exposing photocurable resin to a UV light source which cures and hardens the resin and thus 'prints' each layer of the part, though DLP machines use a projected light source to cure entire layers at once while SLA machines traditionally use a UV laser beam to carefully trace each layer. Masked stereolithography (MSLA) machines, which use an array of UV light sources masked with an LCD screen and cure entire layers at once like DLP, are becoming increasingly popular as they tend to print faster than traditional SLA methods.

Hobby quality vat polymerization devices are available with z-axis resolutions as small as 10 microns, which make them ideal candidates for attempting to print diffraction gratings, the small sizes of which are often necessities. For this project, fork holograms were printed with MSLA, SLA, and FDM printers, to varying degrees of success. Table 1 below details the method, brand, and resolution of each printer used in this project.

Method	Printer	XY Resolution	Z Resolution
MSLA	Elegoo Mars 2 Pro	0.05 mm	0.01-0.2 mm
SLA	Formlabs Form 3+	0.025 mm (0.085 mm Laser Spot Size)	0.025- 0.3 mm
FDM	Prusa i3 MK3S+	0.4 mm*	0.05 -0.35 mm

Table 1. Summary of additive manufacturing method, device, and resolutions. *The xy-resolution of FDM printers like the Prusa i3 MK3S+ are limited by the filament nozzle diameter, of which 0.4 mm is the default and what was used for this project.

Modeling the Gratings

For each desired LG mode, a bitmap image of the inverse of each final grating was converted to a DFX file using LinkCAD. These DFX files were then imported into Autodesk's Fusion360 CAD modeling software as a sketch (though the scale was converted from micron to millimeter) from which a solid body of the hologram was created by utilizing the 'extrude' tool. To ensure the hologram consisted of a single body with a closed build volume, each fringe was manually inspected to verify its connection to adjacent fringes, with additional bodies created and merged as necessary. Once the hologram body was confirmed to have a closed volume, it was re-scaled to the original desired size of 6mm x 6mm x 1mm and exported as a mesh to an STL file, the format required by nearly all 3D printers. Generating the 3D models of a hologram was a tedious and prolonged process, as the number of facets produced by the DFX sketch bogged down the processor on even a robust desktop. Those wishing to follow a similar process may seek a different, more efficient method for generating the 3D models of the holograms.

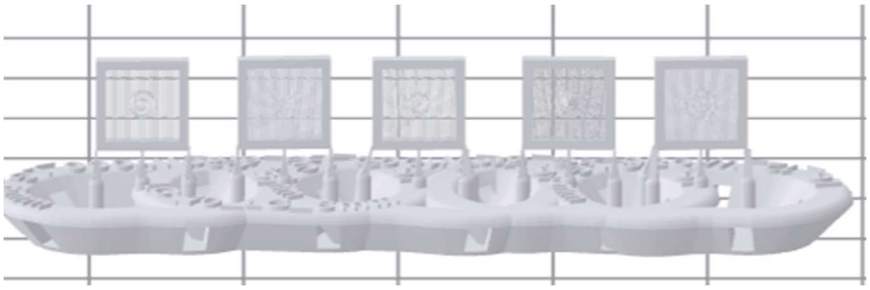

Figure 5. Each hologram modeled for 3D printing. This layout was used specifically for one of the first iterations of holograms printed with the Form 3.

Results

Masked Stereolithography

The first holograms were printed using the Elegoo Mars 2 Pro, a hobby-quality MSLA printer, which boasts, for its cost, an impressive xy-resolution of 50 microns and a z-resolution of as low as 10 microns. Theoretically, this resolution was fine enough (if only just) to print the hologram at the desired 6mm x 6mm x 1mm scale with 60 μm fringes, however the resulting hologram was a solid body with no resolvable fringe features. The holograms were scaled up substantially for the second Elegoo printing attempt to a size of 6cm x 6cm x1cm (10x scale), though all exhibited significant feature warping at this size as shown below in figure 6.

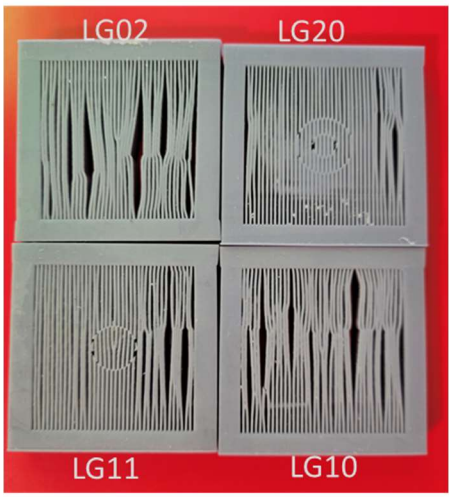

Figure 6. Results of only iteration of holograms printed with Elegoo Mars 2 Pro. Joined and warped fringes present for each mode, though clearly more pronounce in modes with a radial mode p=0.

Cursory visual inspection led to an initial belief that while the LG10 and LG20 holograms were completely useless due to deformities of the fringe structure, the LG11 and LG02 holograms may been usable. Closer investigation, however, revealed large deposits of resin that had been trapped between fringes and subsequently cured, preventing necessary

transmission through the grating. Unfortunately, no further prototypes were made using this printer, though it remains a viable option for use in the future.

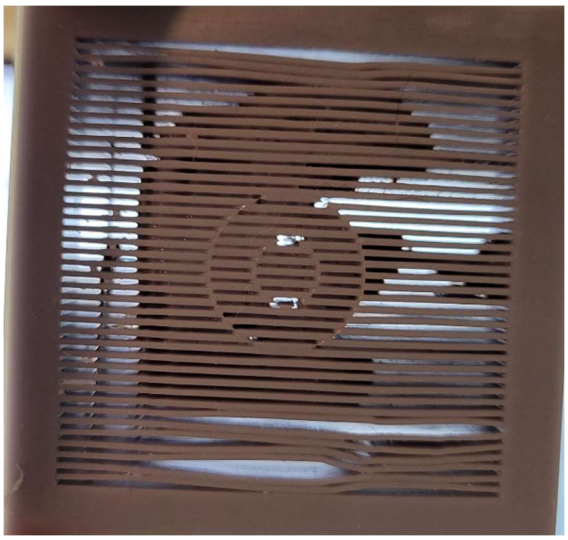

Figure 7. Example of cured resin deposits trapped between features of the LG02 Elegoo printed hologram. Most significant in holograms with $p > 0$.

Stereolithography

A more methodical approach was used for subsequent printing efforts, which focused on determining a realistic scale for holograms printed on the Formlabs Form 3 industrial quality SLA printer, which, like the Mars 2, has a resolution theoretically capable of printing holograms at the originally desired scale, but fails to realize such fine features during the actual printing process. After the initial LG10 print was unsuccessful, the same hologram was printed using clear resin at increasingly large scales until well defined, though not perfect, fringe separation finally occurred at an 8x scale.

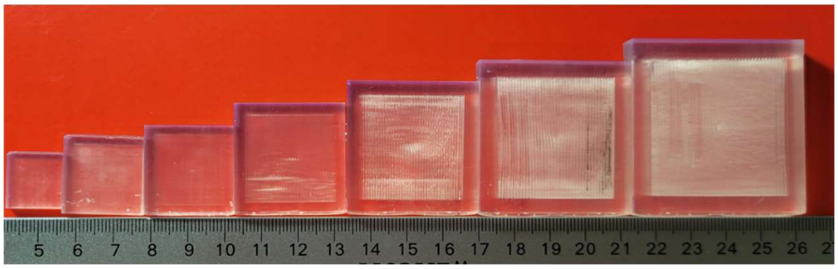

Figure 8. Iterations of LG10 prototype holograms of increasing scale printed by an associate at BlueHalo using the Form 3 printer. Scales range from 2.5x (leftmost) to 8x (rightmost), at which fringe separation was finally achieved.

Having achieved a successful prototype, the following LG20 hologram was printed at this same scale but with opaque white resin for lab testing. Fringe separation was once again accomplished, however was not maintained as well in the LG10 prototype; this is not believed to be caused by any differing physical or chemical qualities of the resins and is thought to be the result of slight curvature in the fringes displaced by the center fork, which grows more pronounced as the number of splits in the fork increases. Efforts to mitigate this and produce a hologram with this printer of high enough quality for lab use are ongoing.

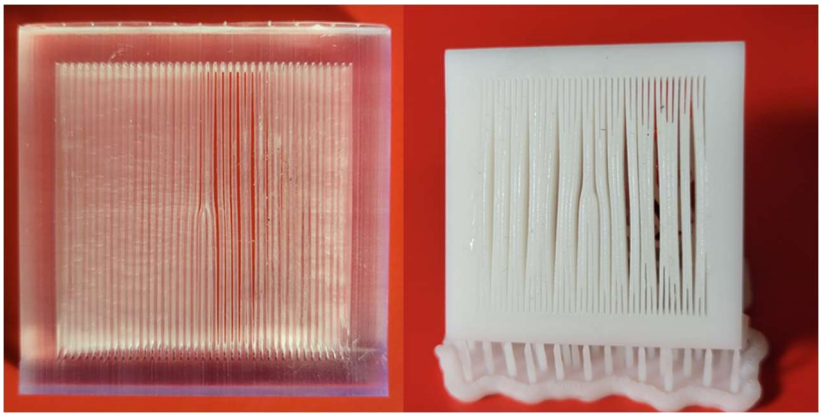

Figure 9. Increase in joined fringes between LG10 (left) and LG20 (right) modes both printed at an 8x scale with the Form 3. Though not clearly visible because of its translucency, the LG10 hologram had only 1 or 2 instances of joined fringes, while not a single fringe remained wholly independent in the LG20 hologram.

Fused Deposition Modeling

Currently, this project's only successfully 3D printed fork hologram was fabricated using the Prusa i3 MK3S+ filament printer for a 10x scale. The initial batch of prints generated by this printer failed due to a misalignment which occurred during the print processes, thought to have been caused by issues with the build volumes of the mesh bodies saved in the STL files used for printing. The files were corrected, however at this point only the LG10 hologram has been printed.

Figure 10. 10x scale Prusa LG10 hologram, mounted for used in the UAH turbulence laboratory.

Lab Results

Preliminary testing of the Prusa LG10 hologram was attempted in one of UAH's interferometry labs with a Mach-Zehnder interferometer, though it was quickly apparent that because of the pronounced size of the hologram, a much larger propagation distance was required to observe any results. Testing was thus moved to the Optical Turbulence lab whose current setup is arranged to allow for a beam to propagate up to approximately 504 feet. For tests of the LG10 Prusa hologram, a spatially filtered and collimated Helium-Neon laser was

diffracted through the hologram and the resulting pattern propagated roughly 126ft, before being reflected and traveling an additional 126ft to an observation screen.

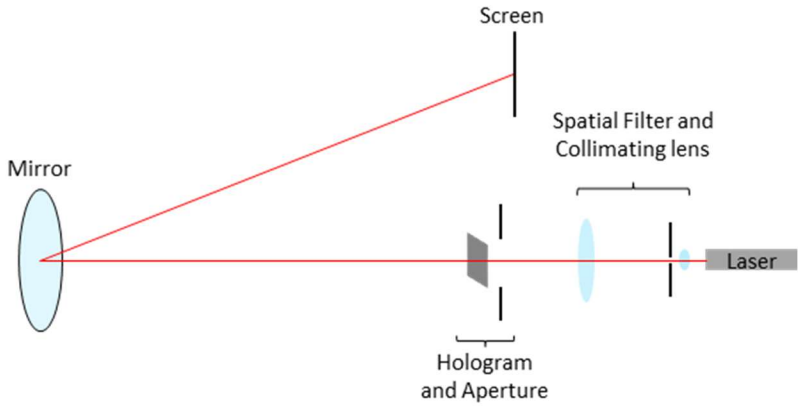

Figure 11. Turbulence lab arrangement used to test the LG10 hologram, not to scale.

Despite initial skepticism, the optical vortices predicted to occur at each diffraction maximum were clearly visible!

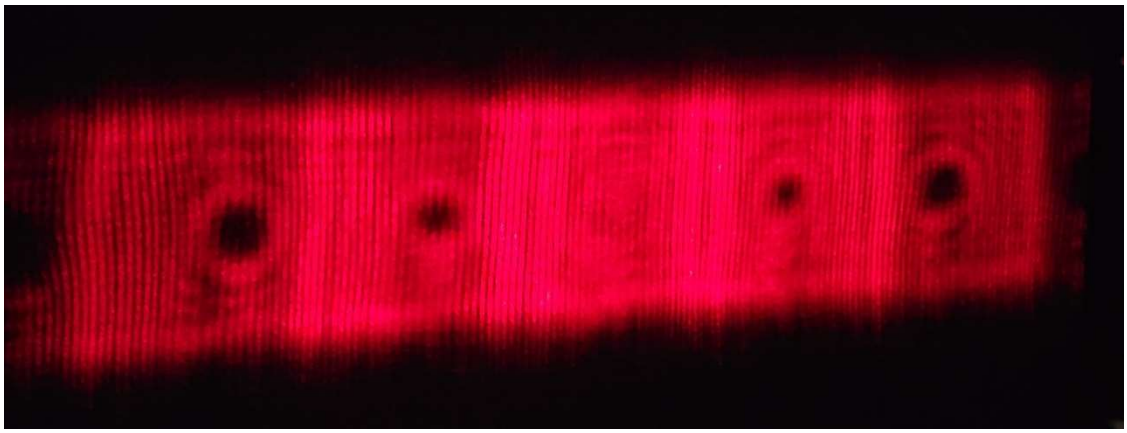

Figure 12. Diffraction pattern of LG10 Prusa hologram after approximately 254 feet of propagation.

Observation of the diffraction pattern along the beam's path revealed that while diffraction phenomena were clearly visible after only 15 feet of propagation (measured from the hologram), optical vortices only began to faintly appear at distance of 60 feet. Immediately before reflection (at 126 feet), the vortices within the diffraction pattern were quite clear, though there was still a

significant amount of overlap between each maximum. Even at a propagation distance of approximately 252 feet, overlap between orders was still present, though each vortex at this point was almost fully isolated. Setup of the turbulence lab allows for a total of about 504 feet of propagation, though pattern propagation at distances beyond 252 feet would be limited to the diameter of reflecting mirrors and has not yet been observed. Setups for observing the hologram's diffraction patterns under conditions of reflection have yet to be attempted.

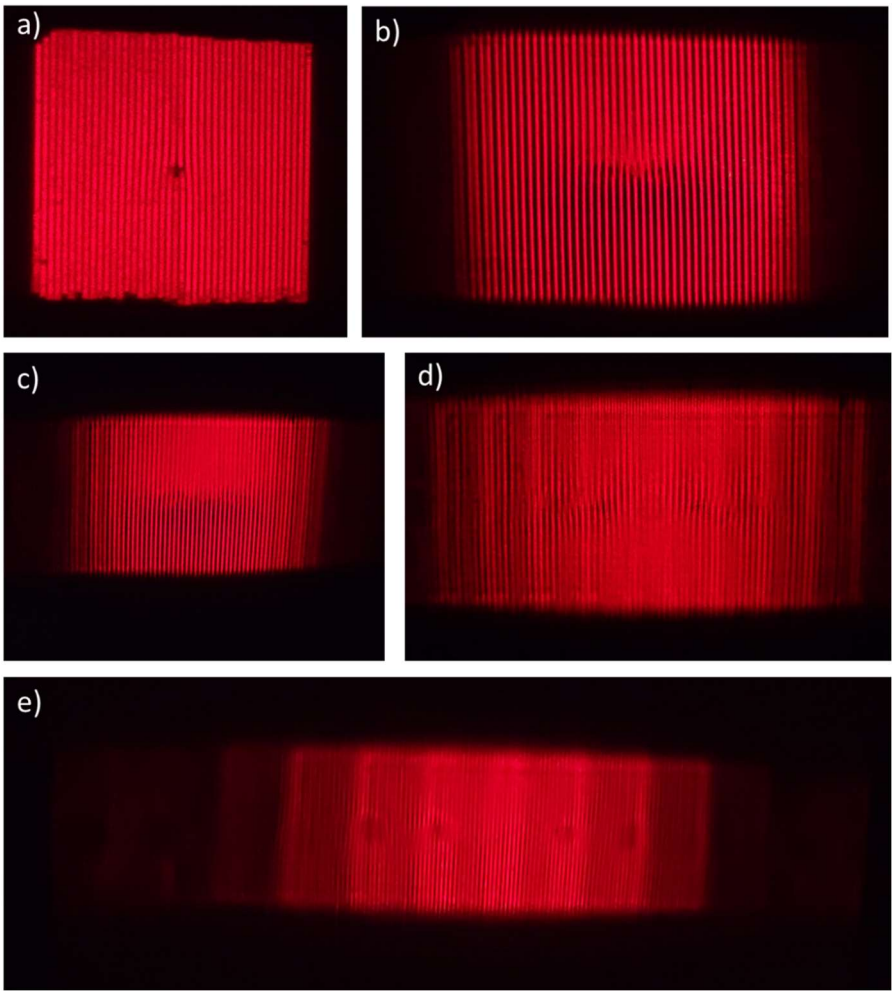

Figure 13. LG10 hologram diffraction pattern at increasing distances. 13.a) shows the beam immediately after passing through the hologram. 13.b) shows the diffracted beam at 15 feet, 13.c) at 30 feet, 13.d) at 60 feet, and 13.e) at 126 feet (immediately before reflection).

Conclusions

For applications which require and/or allow for long propagation distances, fork holograms fabricated via additive manufacturing offer a viable method of optical vortex generation, despite the size at which they must be printed. Because of the significant distance the diffracted beams must travel before enough separation between orders is achieved, any analysis of a vortex's topological charge via the typical interferometry techniques would present a profound challenge.

Of the printing methods explored in this project, the most reliable appears to be traditional filament deposition, however its efficacy when producing higher order LG modes has yet to be examined. The use of stereolithography to produce holograms at slightly smaller scales has considerable potential, however the fringe warping which occurs in LG holograms with $p = 0$ and $\ell > 1$ suggests that SLA may be best used to produce fork holograms with radial modes $p > 0$, due the stability the ring dislocations of higher-order radial modes appear to add to the fringe patterns (inferred from the relative success of the Elegoo LG02 and LG11 modes when compared to the LG10 and LG20 modes from the same batch). Those wishing to develop this project further may wish to attempt FDM printing the holograms at a slightly smaller size, comparing the diffraction patterns resulting from transmission and reflection setups, attempting to generate holograms at higher resolutions, and comparing the diffraction patterns for holograms of the same modes created for different incident beam diameters, among other things.

Ultimately, the ability of such a large, relatively low-resolution fork hologram to produce distinct optical vortices illustrates at the very least, 3D printed fork holograms afford a convenient and low-cost method of testing CGHs before committing to a set design.

Appendix 1: MATLAB Code

Fork Hologram Generator

Honors Capstone, SP 2022
Tara Crowe

```
% Enter Hologram and Interference Parameters

N = 4800; %Dimension of Hologram in microns
Angle1 = asind(0.6328/120); % Angle of plane wave in degrees for a period of 120 um
V=0.5; % Beam Contribution Controller (0.5 indicates each beam has the same amplitude)
L = 1; % Topological charge
P=1; % Radial Mode
lambda=0.6328*1e-6; % Wavelength (He-Ne laser)
W=1000*lambda; % LG Beam Diameter at plane of interference

% Create sample space
del=1*1e-6; % Scale for micron size
x=-N/2:N/2-1;
y=-N/2:N/2-1;
[X,Y]=meshgrid(del*x,del*y);

% Generate LG Beam
r = sqrt(X.^2 + Y.^2);
Phi = atan2(X,Y);
Term1 =(((sqrt(2)*r./W)).^abs(L));
Term2 = polyval(LaguerreGen(P,L),((2.*r.^2)/W^2)); %[11]
Term3 = (exp(-(r.^2)/W^2));
Term4 = (exp(1i*L.*Phi));
Z = A.*Term1.*Term2.*Term3.*Term4;

% Isolate Phase component of LG beam
Phase = angle(Z);

% Create LG object wave
LG = 0.5*exp(1i*(Phase));

% Create tilted plane reference wave
B=0.5*exp(1i*(2*pi/lambda)*tand(Angle1)*(X));

% Simulate interference between object and reference wave
intf_patt = LG+B;
hgram = abs(intf_patt).*abs(intf_patt); %Intensity of Interference Patten 1

% Generate Fork hologram
inv_mask=imbinarize(hgram);%Binarized intensity
hologram = ~(inv_mask);

% Inverted mask for conversion to DFX
inv_mask_border = padarray(inv_mask,[600,600],1,'both');
```

```
% Hologram mask for viewing
hologram_border = padarray(hologram,[600,600],0,'both');

% Convert inverse mask to phase grating
% Increases diffraction efficiency into m = 1 and m = -1 diffraction maxima
% [12]
phase_grating = exp(1i*pi*inv_mask);

% Zero-padd phase grating
% Effectively decreases spatial frequency of grating to enhance resolution
% of diffraction pattern
zp_grating = padarray(phase_grating,[600,600],0,'both');

% Optionally display hologram resul
figure
imagesc(hologram_border);

% Optionally save inverted mask and/or hologram
imwrite(inv_mask_border,'INV_L1P1_paper_example.bmp');
imwrite(hologram_border,'L1P1_hologram_example.bmp');


% Simulate Diffraction
E = fftshift(fft2(zp_grating)); %Modeling Far Field Diffraction pattern
E_int = (abs(E)/(N*N)).*(abs(E)/(N*N)); %Intensity

figure
imagesc(E_int);
title(' Simulated Diffraction Pattern')
```

References

[1] Y. Shen, X. Wang, Z. Xie, C. Min, X. Fu, Q. Liu, M. Gong, and X. Yuan, "Optical vortices 30 years on: OAM manipulation from topological charge to multiple singularities," *Light: Science & Applications*, vol. 8, no. 1, 2019.

[2] M. Padgett, J. Courtial, and L. Allen, "Light's Orbital Angular Momentum," *Physics Today*, vol. 57, no. 5, pp. 35–40, May-2004.

[3] A. V. Carpentier, H. Michinel, J. R. Salgueiro, and D. Olivieri, "Making optical vortices with computer-generated holograms," *American Journal of Physics*, vol. 76, no. 10, pp. 916–921, Oct. 2008.

[4] S. Maji and M. M. Brundavanam, "Topological transformation of fractional optical vortex beams using computer generated holograms," *Journal of Optics*, vol. 20, no. 4, p. 045607, 2018.

[5] L. Carbone, C. Bogan, P. Fulda, A. Freise, and B. Willke, "Generation of high-purity higher-order Laguerre-Gauss beams at high laser power," *Physical Review Letters*, vol. 110, no. 25, 2013.

[6] L. Carbone, P. Fulda, C. Bond, F. Brueckner, D. Brown, M. Wang, D. Lodhia, R. Palmer, and A. Freise, "The generation of higher-order Laguerre-Gauss optical beams for high-precision interferometry," *Journal of Visualized Experiments*, no. 78, 2013.

[7] S. Li and Z. Wang, "Generation of optical vortex based on computer-generated holographic gratings by photolithography," *Applied Physics Letters*, vol. 103, no. 14, p. 141110, 2013.

[8] J. Arlt, K. Dholakia, L. Allen, and M. J. Padgett, "The production of multiringed laguerre–gaussian modes by computer-generated holograms," *Journal of Modern Optics*, vol. 45, no. 6, pp. 1231–1237, Jun. 1998.

[9] S. Topuzoski and L. Janicijevic, "Fraunhofer diffraction of a laguerre–gaussian laser beam by fork-shaped grating," *Journal of Modern Optics*, vol. 58, no. 2, pp. 138–145, 2011.

[10] L. D. Vallejo Melgarejo, J. García, R. G. Reifenberger, and B. Newell, "Manufacture of lenses and diffraction gratings using DLP as an additive manufacturing technology," *Volume 2: Mechanics and Behavior of Active Materials; Structural Health Monitoring; Bioinspired Smart Materials and Systems; Energy Harvesting; Emerging Technologies*, 2018.

[11] Mattthias Trampisch (2022). Generalized Laguerre polynomial (https://www.mathworks.com/matlabcentral/fileexchange/15916-generalized-laguerre-polynomial), MATLAB Central File Exchange. Retrieved May 2, 2022.

[12] S. Bhattacharya and A. Vijayakumar, *Design and fabrication of Diffractive Optical Elements with MATLAB®*. Bellingham, WA: SPIE Press, 2017.